OPTICA

X-ray parametric down-conversion at an XFEL

Nicholas J. Hartley,[1,2,*] **James Baxter,**[1] **Scott Curtis,**[3] **Okhura Daisuke,**[4] **Aliaksei Halavanau,**[1] **Abigail H. Carpenter,**[3] **Janita Hussain,**[1] **Taito Osaka,**[5] **Norimasa Ozaki,**[4] **Richard L. Sandberg,**[3] **Sharon Shwartz,**[6] **Kai Taketoshi,**[4] **Naoki Yamagata,**[4] **and Siegfried H. Glenzer**[1]

[1]*SLAC National Accelerator Laboratory, Menlo Park, California 94025, USA*
[2]*Open and Transdisciplinary Research Institute, Osaka University, Suita, Osaka 565-0871, Japan*
[3]*Department of Physics and Astronomy, Brigham Young University, Provo, Utah 84602, USA*
[4]*Graduate School of Engineering, Osaka University, Suita, Osaka, Japan*
[5]*Japan Synchrotron Radiation Research Institute (JASRI), Sayo-cho, Hyogo, Japan*
[6]*Physics Department and Institute of Nanotechnology, Bar-Ilan University, Ramat Gan 52900, Israel*
*njh@slac.stanford.edu

Understanding and harnessing X-ray quantum effects could open new, to our knowledge, frontiers in imaging and quantum optics. In this study, we measured the process of X-ray parametric down-conversion, where a single high-energy X-ray photon splits into two lower-energy photons. Using the SACLA X-ray free electron laser in Japan at 9.83 keV, we found clear evidence that pairs of photons were produced along the energy-angle relationship that conserved both energy and momentum, as predicted for down-conversion, and consistent with quantum entanglement of X-ray photons. By matching specific photon pairs for energy and momentum conservation, we observe a signal rate of 1250 pairs per hour, confirming that correlated photon pairs can be generated and observed in the absence of explicit time correlations. Our results show that with further refinement, the number of entangled photons produced per laser pulse could increase by an order of magnitude. This paves the way for demonstrating quantum-enhanced X-ray imaging, and confirmation of X-ray photon entanglement.   © 2025 Optica Publishing Group under the terms of the Optica Open Access Publishing Agreement

1. INTRODUCTION

Correlated photon pairs are an explicit manifestation of the quantum properties of light. Although such pairs have been generated and observed across the electromagnetic spectrum, most of the work has focused on producing optical photons, where they have been used to observe photon entanglement [1,2]. Such pairs of photons can be generated by spontaneous parametric down conversion (SPDC), a nonlinear, quantum optical process [3–5] in which a single high-energy ("pump") photon elastically produces a pair of lower-energy photons (generally termed the "signal" and "idler"). In the optical regime, this process was first observed using nonlinear (birefringent) crystal [6,7]. The resulting photon pairs have been demonstrated to show properties of quantum entanglement, including violating the Bell inequalities [1,8].

This same process has been observed in the X-ray regime at synchrotron facilities [9–13]. In this case, a traditional nonlinear crystal is replaced by a high-quality low-Z crystal [14,15], where a plasma-like nonlinearity can be excited close to a Bragg peak [16]. This nonlinearity is achieved because the incoming X-rays have a significantly higher energy than the binding energies of the electrons with which they interact. This was verified in 1971 using scintillator detectors and a Mo-Kα source [17], which observed down-converted pairs at a rate of around 1 pair/h. More recent

experiments using a similar approach have increased this to around 90 pairs/h [9], and increasing observation rates continues to be an active area of research [13]. Even these low rates are significantly larger than those from other proposed approaches to pair production, such as quantum vacuum fluctuations [18], nuclear forward scattering [19], or direction generation within free-electron lasers [20].

Although this spontaneous process occurs with low probability, possible applications for such correlated X-ray pairs have been proposed, primarily as a way of increasing the signal for imaging or probing. The correlations between the photons allow for analysis that can reduce background [21], increase signal-to-noise [11], and decrease the required on-sample dose [10]. For fragile samples where high doses destroy the sample as they image it [22,23], this would allow non-destructive imaging with much higher resolution [24]. Such pairs would also allow quantum optics studies at X-ray wavelengths. The Hong-Ou-Mandel interference effect was originally demonstrated with optical SPDC pairs [25] and would confirm X-ray photon entanglement [26], as is predicted for these down-converted photon pairs [27]. Other work has shown how entangled optical pairs can open up entirely new spectroscopic methods to probe interactions of biological samples with light [28,29], and extending this to X-rays would be similarly exciting.

In this work, we have demonstrated X-ray SPDC at the SACLA X-ray free electron laser (XFEL). A clear excess signal is observed along the energy-angle relationship, fulfilling the energy- and momentum-conservation requirements of down-conversion. After photon matching, we have determined a rate of 1250 pairs observed per hour, which could reach over 10,000 entangled pairs per hour with improvements to the experimental setup. This could then be increased to over 100,000 per second, in proportion to the repetition rate, at an MHz facility such as LCLS-II-HE [30].

2. PARAMETRIC DOWN-CONVERSION

The process of X-ray parametric down-conversion by Bragg detuning is described in more detail in previous work [17], but a brief summary is reproduced here. We initially consider a perfect crystal set up to diffract an incoming photon with energy $E_p = \hbar \omega_p$ and corresponding wavevector $\vec{k}_p = 2\pi/\lambda_p = E_p/\hbar c$, with c as the speed of light, and pointing along the direction of propagation. These equations assume that the refractive index in all of the media is unity, such that the wavenumber, $|k_p|$, is directly proportional to the energy; in the hard X-ray regime, this introduces errors of order 10^{-5}. The outgoing beam then has wavevector $\vec{k}_o$, shown in Fig. 1(a), with $|\vec{k}_o| = |\vec{k}_p|$, such that this is an elastic interaction.

For down-conversion to occur, the perfect crystal can be detuned by a small angle $\delta\theta$, as shown in Fig. 1(b). Energy and momentum conservation can then instead be met by the production of a pair of photons that satisfy the phase-matching conditions around the Bragg peak $\langle hkl \rangle$. From conservation of momentum, we require

$$\vec{k}_p + \vec{G}_{hkl} = \vec{k}_s + \vec{k}_i \tag{1}$$

and from conservation of energy

$$\left| \vec{k}_p \right| = \left| \vec{k}_s \right| + \left| \vec{k}_i \right|. \tag{2}$$

The subscripts p, s, and i, indicate the incoming (pump) and outgoing (signal and idler) photons, respectively, with G_{hkl} as the wavevector of the Bragg peak. Together, these describe two photons being produced with energies that sum to that of the incoming photon $E_p = E_s + E_i$.

In the case where the misalignment $\delta\theta$ is small, the angle between the emitted signal (or idler) photon and the Bragg angle, designated $R(E_s)$, can be well-approximated by [14,15,17]

$$R(E_s) = \sqrt{2\delta\theta \left(\frac{E_p - E_s}{E_s} \right) \sin 2\theta_B}, \tag{3}$$
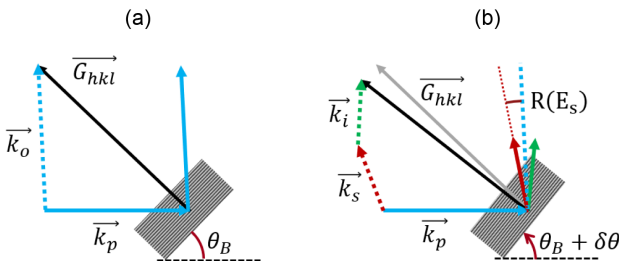

Fig. 1. Schematic illustration of pump-crystal interaction in the case of (a) Bragg diffraction and (b) parametric down-conversion, around the crystal reciprocal lattice vector with Miller Indices $[hkl]$. In the latter case, signal and idler photons are produced, with wavevectors $\vec{k}_s$ and $\vec{k}_i$. The dotted lines indicate the vector calculations. Fig. 1 is adapted from [12].
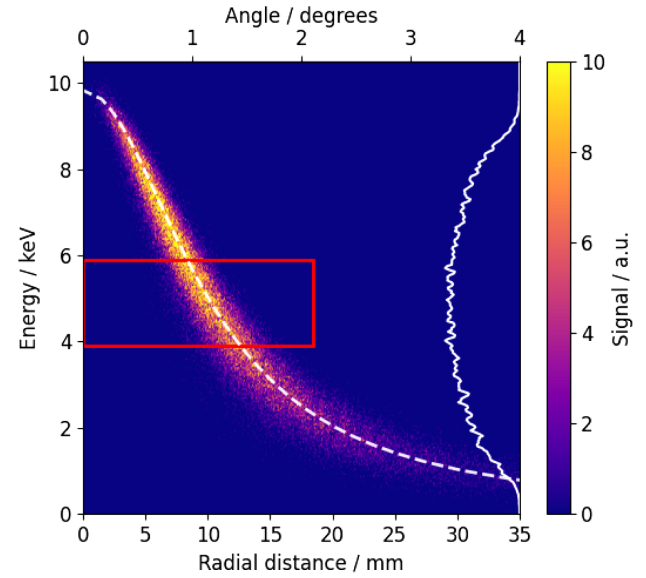

Fig. 2. Simulated down-conversion data, assuming an energy spread of $\Delta E/E = 1 \times 10^{-4}$. The outline shows the coverage analyzed in this experiment, and the dashed line shows the expected radial distance for each energy, r_{exp}, defined in Eq. (4). The solid line shows the total signal at each photon energy, demonstrating the higher probability of down-conversion near to an even energy split.

$$r_{\mathrm{exp}} = d \tan[R(E_s)], \tag{4}$$

where r_{exp} is then the distance of the photon from the center of a detector centered on the Laue peak, depending on the crystal-detector distance, d.

Any energy distribution between the two photons is possible. From Eq. (3), we can see that the higher-energy photon of the pair will be emitted closer to the diffraction peak and would therefore be detected closer to the center of the detector. This expected relationship between the energy of a down-converted photon and its detector position is shown in Fig. 2 and serves as a condition to determine whether a pair of photons could be produced by down-conversion.

For a given detuning angle $\delta\theta$ and a fixed pixel size, the theory suggests that the probability of a given energy split scales as

$$P(E_s) \propto [R(E_s) + R(E_i)]^{-2} \tag{5}$$

such that the most likely event is an energy split close to 50/50, although this effect only becomes significant for highly asymmetric energy splits [31], as can be seen from the solid line in Fig. 2. The total probability of down-conversion should not vary with crystal misalignment [17], in agreement with results from our previous work [12].

3. EXPERIMENTAL DETAILS

Our experiment used the SACLA XFEL BeamLine3 [32] at a photon energy of 9.83 keV ($\lambda = 1.27$ Å). This was self-seeded for an FWHM bandwidth of roughly 5 eV, which was further reduced to 1 eV by passing the beam through a 4-bounce silicon-(111) monochromator. The seeded beam fluence was measured as 280 ± 30 µJ/shot, which we calculate was reduced to around 20 µJ/shot (1.27×10^{10} photons/shot) by passage through

the monochromator. This is much less than the ideal reflectivity due to an offset of 5 eV between the peak of the seeded pulse and the monochromator angle. The beam was incident onto a 100-oriented single crystalline diamond target ($5 \times 5 \, \text{mm}^2$, 109 µm thick), initially aligned for the beam to Bragg diffract off the [400] lattice plane (parameter $\vec{G}_{400} = 7.040 \, \text{Å}^{-1}$), through an angle of $\theta_B = 45.1°$, in the horizontal plane. Since the incoming X-ray beam is horizontally polarized, the Bragg and Compton scattering will be strongly suppressed, by a factor of $1 - (\sin \theta_B \cos \phi)^2 = 2.4 \times 10^{-4}$, relative to scattering in the vertical plane [33].

In order to observe parametric down-conversion, we detuned the diffraction angle by 12 mdeg, as well as taking data with a negative detuning of 30 mdeg for a background (null) signal. With $\delta\theta = 12$ mdeg, we can use Eq. (3) to estimate the emission angle. In the degenerate case ($E_s = E_i$), where both photons are at 4.9 keV, they will be emitted 1.2° on either side of the Bragg peak, while other energy splits will follow the relation described above. The expected angular relationship, convolved with blurring effects from the energy spread and angular variation measured in this experiment, can be seen in Fig. 2.

As shown in Fig. 3, the photons are detected on a multi-port charge couple detector (MPCCD) located 50 cm from the interaction point. At this distance, the phase-matching angle for degenerate photons corresponds to just over 1 cm from the diffraction peak position, or 205 pixels. The detector response was initially calibrated by placing titanium and iron foils in the beam in order to generate Kα emission (at 4.51 and 6.41 keV, respectively). Fitting to these peaks allowed a pixel-by-pixel calibration of the signal to photon energy on the device. This also allowed us to estimate the uncertainty in the energy measurement, which was normally distributed with $\sigma_E = 0.6$ keV. Before calibration, we used a droplet algorithm to find the total signal in cases where the absorbed energy was spread between adjacent pixels. A lower signal cutoff of 21 adu (corresponding to around 2 keV) was applied in order to reduce noise on the detector.

The target and detector were both located in the air, but the attenuation length for 4.9 keV X-rays in the air is around 20 cm, so in order to increase the signal collection efficiency, we added a beam tube, sealed with 20 µm PET (Mylar) windows on either end
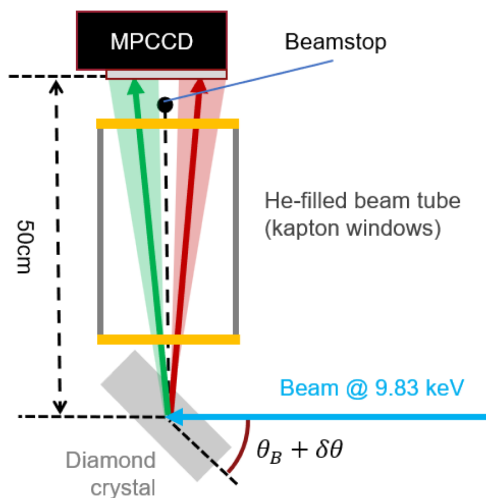

Fig. 3. Schematic of the experimental setup, with the XFEL beam incident onto a detuned diamond crystal. The down converted photons (red and green) pass through a helium-filled beam tube to the MPCCD detector located 50 cm away from the interaction point.

and pumped with helium. The remaining path in the air was estimated at 5 cm, with further losses due to the quantum efficiency of the detector and potential absorption within the diamond crystal. Combining these effects, we can estimate an energy-dependent total transmission factor $p_t(E_s)$. In the degenerate case, $p_t(4.9 \, \text{keV}) = 0.499$, implying that 24.9% of the degenerate pairs produced would be visible on the detector. The transmission factor rapidly decreases for lower energies, primarily due to the remaining air path, meaning that more asymmetric energy splits have a lower chance of observation. Over the energy range analyzed below (3.9–5.9 keV), and weighted by the probability of a given energy split $P(E_s)$, the average probability of both photons reaching the MPCCD and being detected is 21.8%, due to a combination of absorption and detector quantum efficiency. We can therefore define an averaged transmission for the analysis of $\overline{p_t} = 0.466$.

4. PAIR FINDING

In our previous work at the APS synchrotron [12], we were able to confirm down-converted pair generation by looking for a peak in time-energy correlation space: if a photon with half of the energy of the pump is seen at the predicted angle from the Bragg peak, another with the same energy should also be seen directly opposite it at the same time. This relies on a coincidence counter, together with a quasi-continuous incoming X-ray beam and a very high efficiency of photon detection, which was possible due to usage small-area silicon drift detectors.

At an XFEL, such an approach is not possible. Although the average photon flux per second is similar, the photons are delivered in femtosecond-scale bunches, such that we cannot rely on time-energy correlation. Instead, we can determine the presence of a down-converted signal by using an area detector and looking for the expected relationship between the energy and position of a given photon, as plotted in Fig. 2.

For each detected photon, we can compare its distance from the center of the detector, r, to the position expected for its energy, r_{exp}, as defined in Eq. (4). Figure 4(a) shows the two-dimensional histogram of signal, binned by energy and the normalized radius, r/r_{exp}, in the case of negative detuning ($\delta\theta = -30$ mdeg), integrated over 1.5×10^5 shots (around 1.5 h at 30 Hz). This dataset serves as a background since down-conversion is not possible for this detuning. We can see that, even in this case, there is a large amount of signal close to $r/r_{\text{exp}} = 1$, i.e., where we would expect to see the down-converted signal. In order to distinguish this smaller down-converted signal above the background, Figs. 4(b) and 4(c) show the same histogram for the case of $\delta\theta = 12$ mdeg, with the normalized background subtracted to show the excess signal. The limited energy range is chosen primarily due to the large increase in detector noise at lower energies and to be symmetric about the degenerate energy split at 4.9 keV.

To find correlated pairs, we analyze each possible pair of photons i, j in each shot. Possible pairs are those that fulfill:

- $E_i + E_j = 9.83 \pm \Delta E$, requiring the photons to conserve the incoming energy, and
- $\varphi_i + \varphi_j = \pi \pm \Delta\varphi$, requiring the photon pair to be emitted symmetrically around the diffraction peak at the detector center, for momentum conservation.

In both cases, the total is accurate with some uncertainty ΔE and $\Delta\varphi$. For this analysis, we used values $\Delta E = 0.94$ keV and
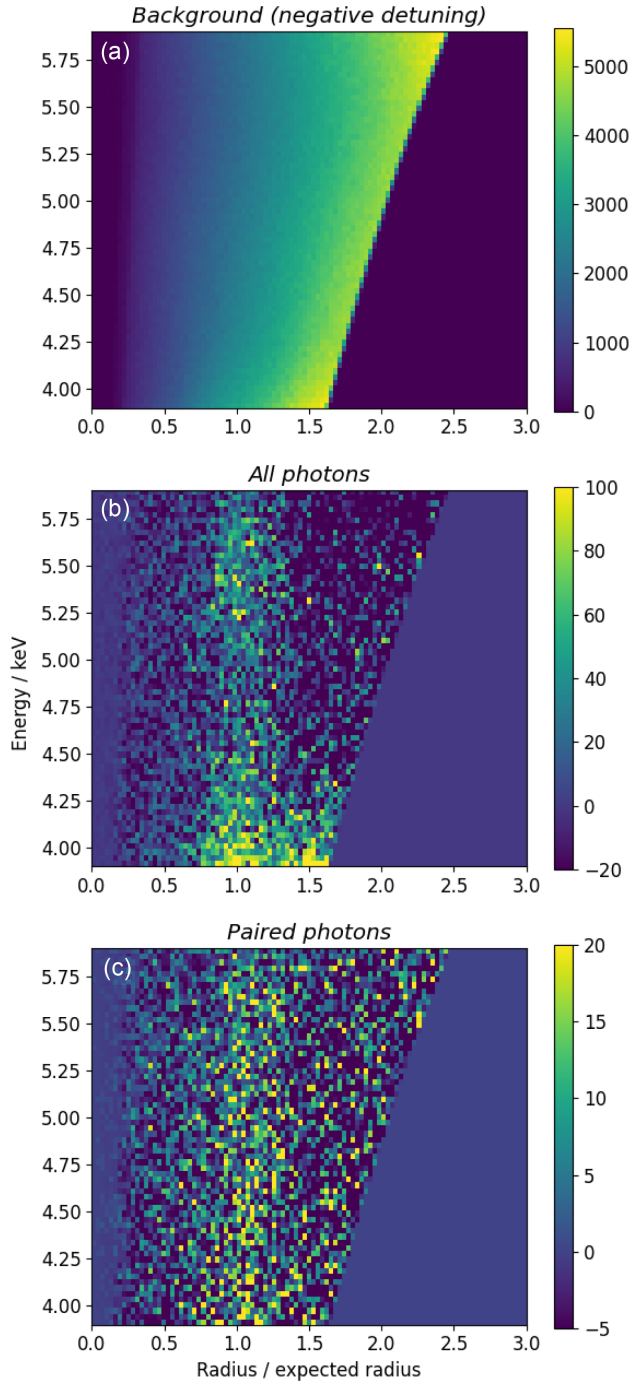
Fig. 4. Observed signal as a function of photon energy versus distance from detector center, relative to the expected distance for that energy. (a) Shows the background signal, with the crystal detuned to negative angles, such that down-conversion is not possible. The lower two images show the excess signal over that background with positive detuning ($\delta\theta = 12$ mdeg) before, (b), and after, (c), photon pair-finding. In both, the peak at $r/r_{\exp} = 1$ corresponds to down-converted photons. The color bar represents photons per bin—note the difference for each figure.

$\Delta\varphi = 12.8$ mrad, which we will see below maximize the proportion of paired photons on the detector. Images of the excess photon distributions before and after performing the pair-finding analysis are shown in Figs. 4(b) and 4(c).

The emission angles of the photons, and hence the momentum matching condition, depend on an accurate center position. Since the diffraction peak was blocked to reduce signal on the detector, the center position was fine-tuned by maximizing the sharpness of the pair peak for a range of center offsets.

Figures 5(a) and 5(b) show the total data lineouts as a function of normalized radius, integrated over the energy range shown, before and after pair finding. In both cases, the background (negative detuning data) is normalized to the signal. The background-subtracted lineouts, in 5(c) and 5(d), show the clear excess peak. All of the lineouts are cut off at $r/r_{\exp} = 1.6$ as this is the greatest point at which there is a signal for all analyzed energies and are summed over 2 h of shots taken at 30 Hz (2.14×10^5 shots total).

Before pair matching, we have a total of 2.90×10^6 photons on the detector, (13.6 photons per shot); of these, 32,651 photons are located in the excess peak around $r/r_{\exp} = 1$, corresponding to 0.15 photons per shot, or 1.12% of the signal on the detector. The height of the peak over the background is greater than $10\times$ the standard deviation in the background signal.

After pair matching, we see in Fig. 5(b) that the signal still has a clear background which is fitted well by the negative detuning data. Including this background signal, we have a total of 59,500 photons on the detector (0.28 photons per shot). The excess signal peak seen in Fig. 5(d) is 6σ above the background noise level and contains 4986 photons (0.023 per shot), for a total of 2493 confirmed photon pairs produced in the experiment. This is 8.39% of the paired signal on the detector and corresponds to an observed pair every 86 shots, or 1258 pairs per hour. From the incoming photon rate, this corresponds to one observed pair for every 1.09×10^{12} photons incident onto the crystal.

From the ratio of photons in the peak before and after performing pair finding, we can calculate the total efficiency of the transmission and detection and compare it to the value estimated above. First, we need to account for pairs where one or both of the photons falls outside the analyzed energy range. We assume that the pair energies are distributed as described in Eq. (5) and that the measured energy values are normally distributed with $\sigma_E = 0.6$ keV. This reduces the expected pair number by a factor of $f_{\rm in} = 0.655$, i.e., for 34.5% of the "signal" photons in the $r/r_{\exp} = 1$ peak, the corresponding "idler" photon falls outside the analyzed energy range, and so cannot be correctly paired.

We define N as the rate of production of pairs where at least one photon is observed within the energy range of interest. The number of photons in the unpaired peak, shown in Fig. 5(c), is equal to $2Nf_{\rm in}\overline{p_t} + N(1 - f_{\rm in})\overline{p_t}$, with $\overline{p_t}$ as the average transmission defined above. The first term accounts for pairs with both photons detected in the energy range, hence the factor 2 to count both photons, while the second term accounts for unpairable photons. The total number of paired photons within the paired excess peak, in Fig. 5(d), is then equal to $2Nf_{\rm in}(\overline{p_t})^2$; the factor 2 again accounts for both photons in the pair, and the squared transmission factor describes both photons reaching the detector.

Combining these expressions with the calculated value of $f_{\rm in}$, our photon numbers imply an average transmission of $\overline{p_t} = 0.193$, lower than the value of 0.466 estimated above. This suggests that there is either additional absorption of the generated photons, beyond what is accounted for, or that our pair-matching algorithm is not able to identify all pairs where both photons are detected on the MPCCD. Nevertheless, from these values of $\overline{p_t}$, we can estimate the actual rate of down-converted pair production, $N = 27,300 \pm 18,000$ pairs per hour, with the large uncertainty

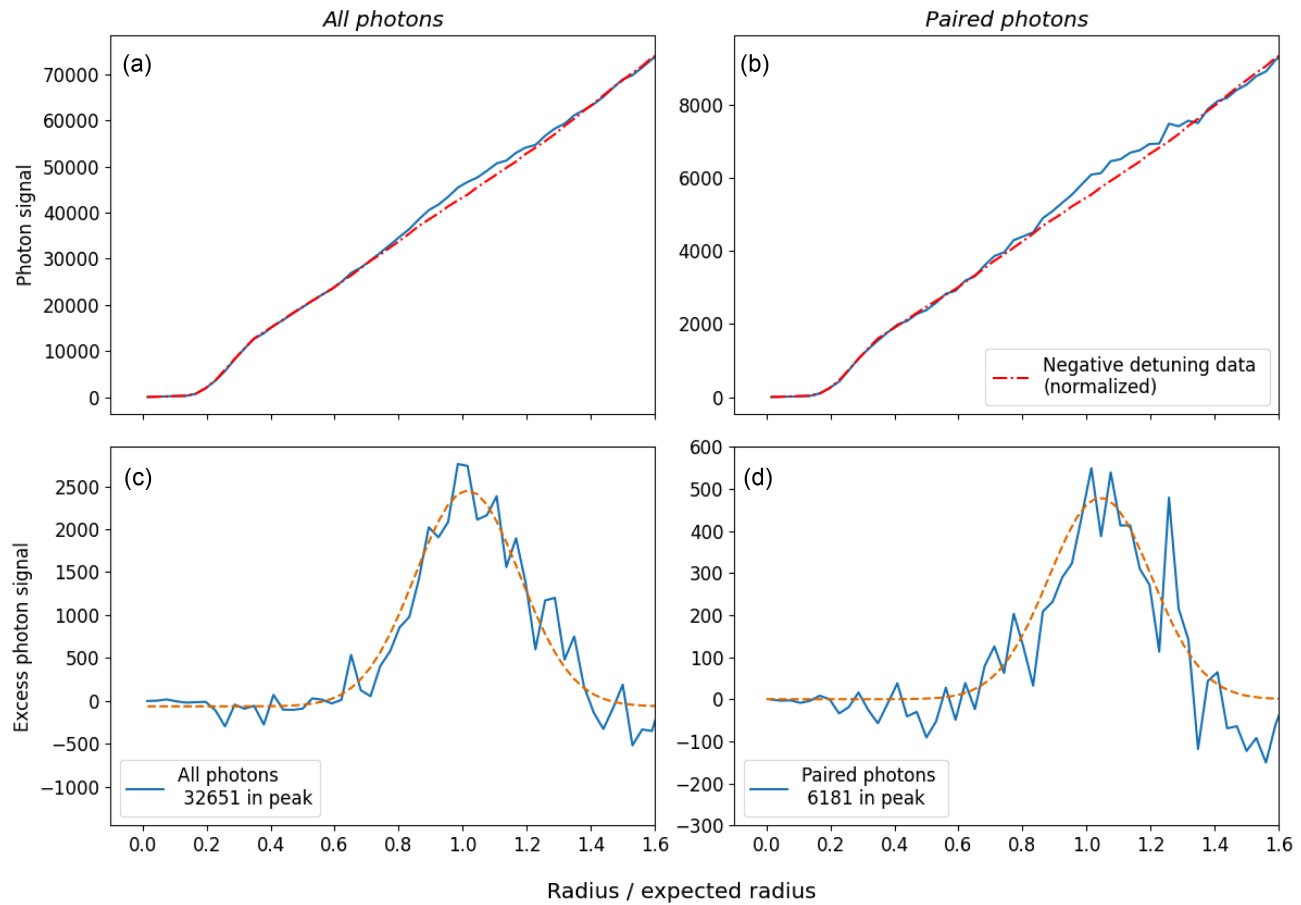**Fig. 5.** Signal histograms as a function of normalized radius (r/r_exp), across the energy range 3.9–5.9 keV. The upper figures show the signal for all photons, in (a), and paired photons, in (b), with the background (negatively detuned) signal normalized to each. The lower figures show the difference between the signal and background in the respective upper figures. The Gaussian peak is fitted to the excess signal from down-converted pairs as a guide to the eye.

coming from the disparity between the calculated and observed transmission. Together with the incoming photon rate, this corresponds to a conversion efficiency of $1.99 \pm 1.31 \times 10^{-11}$, in line with other recent results [13].

The number of pairs identified by our algorithm is greatly affected by the angular and energy acceptance windows, $\Delta\varphi$ and ΔE. Figure 6 shows what percentage of paired photons are located within the central peak as these are varied. The weaker dependence on ΔE is expected due to the large uncertainty in photon energy, while errors in $\Delta\varphi$ come primarily from the beam footprint on the crystal, as well as minor effects from the divergence of the XFEL beam and errors in the detected photon position. As mentioned above, our pair-finding analysis was performed with acceptance values that maximize the pair percentage on the detector, indicated by dotted lines in Fig. 6. A wider angular acceptance $\Delta\varphi$ would increase the number of photons in the excess peak, but only by greatly increasing the total photon numbers on the detector.

In all cases, the low ratio of paired photons to total detector signal ($<10\%$) makes it clear that better energy resolution and lower noise are necessary in order for down-converted pairs to be distinguished more clearly. Better energy resolution would additionally allow the expected energy dependence to be observed, with a decreasing signal at more asymmetric energy splits, further increasing confidence that the measurements are in agreement with the expected down-conversion behavior.

5. CONCLUSION AND FUTURE PROSPECTS

We have observed the production of down-converted X-ray pairs at the SACLA XFEL. In total, we confirmed the observation of 2500 pairs at a rate of around 1250/hour, corresponding to a pair every 85 shots. We additionally see a large excess signal of unpaired photons along the expected energy vs. radius relationship, implying that many more photon pairs are being produced. Our results suggest that pair production rates as high as 20,000 per hour could be observed in a setup with lower losses, such as with the sample and detector in a vacuum, or with reduced noise, allowing photons to be more precisely resolved on the detector.

On a $(100 \text{ pixel})^2$ detector, and assuming that an image can be formed with 10 photons/pixel—for a relatively high-contrast sample, and with quantum-enhanced photon counting—the source reported here could produce an image with a 60 h integration time. With the improvements discussed here and with a 100 Hz facility, this could be reduced to a few hours. In the future, the new LCLS-II-HE XFEL facility will deliver X-rays up to 13 keV at 1 MHz, allowing such an image to be built up in under a second and opening the door to imaging low contrast sample with low enough dose rates to prevent damage. This would also be a strong source for studying X-ray quantum optics. Single heralded photons [11,34] and quantum interference of photon pairs [35] have already been demonstrated with X-rays, and polarization entanglement has been theoretically predicted (e.g., [27]). However, while the SPDC process has been confirmed to generate entangled photon pairs
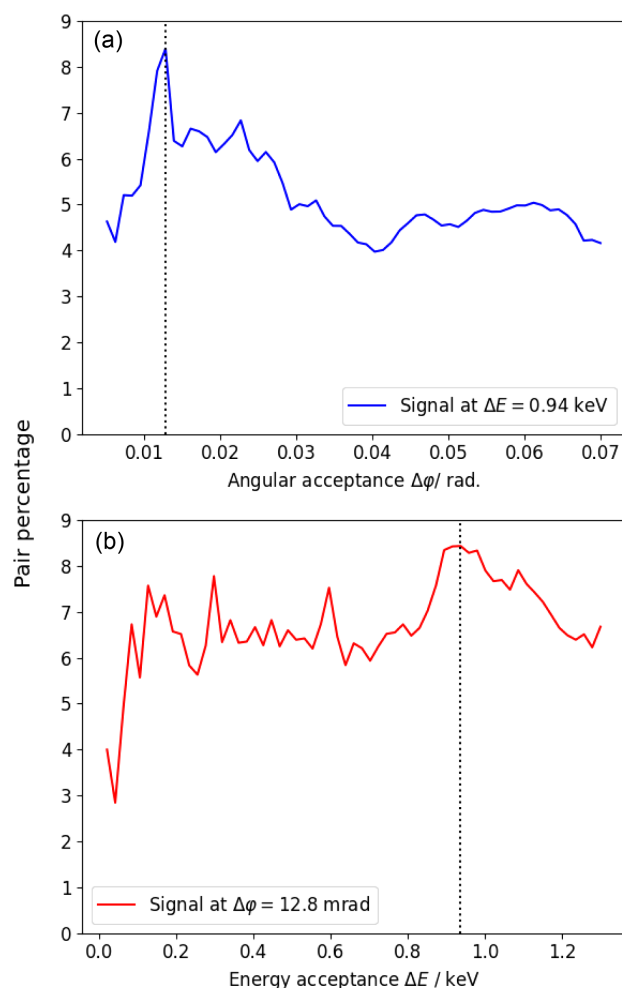
Fig. 6. Proportion of paired photons located within the $r/r_{exp} = 1$ peak as a function of (a) energy and (b) angular acceptance window in the pair finding algorithm. As expected, this peaks at low angular acceptance, with a broader energy dependence, due to the large uncertainty in energy on the detector. The dotted lines indicate the values where the pair percentage is maximized, which are used for analysis.

at optical wavelengths, further experiments are still needed to confirm such entanglement in the X-ray regime.

REFERENCES

1. P. G. Kwiat, K. Mattle, H. Weinfurter, *et al.*, "New high-intensity source of polarization-entangled photon pairs," Phys. Rev. Lett. **75**, 4337 (1995).
2. A. Yoshizawa and H. Tsuchida, "Violation of Bell's inequality in 1550 nm band without subtraction of accidental coincidences," Jpn. J. Appl. Phys. **44**, L375 (2005).
3. M. O. Scully and M. S. Zubairy, *Quantum Optics* (Cambridge University 1997).
4. C. C. Knight and P. L. Gerry, *Introductory Quantum Optics* (Cambridge University, 2007).
5. D. F. Walls and G. J. Milburn, *Quantum Optics* (Springer, 2008).
6. S. E. Harris, M. K. Oshman, and R. L. Byer, "Observation of tunable optical parametric fluorescence," Phys. Rev. Lett. **18**, 732 (1967).
7. D. Magde and H. Mahr, "Study in ammonium dihydrogen phosphate of spontaneous parametric interaction tunable from 4400 to 16 000 Å," Phys. Rev. Lett. **18**, 905 (1967).
8. J. S. Bell, "On the Einstein Podolsky Rosen paradox," Phys. Phys. Fizika **1**, 195 (1964).
9. S. Shwartz, R. N. Coffee, J. M. Feldkamp, *et al.*, "X-ray parametric down-conversion in the Langevin regime," Phys. Rev. Lett. **109**, 013602 (2012).
10. A. Schori, D. Borodin, K. Tamasaku, *et al.*, "Ghost imaging with paired x-ray photons," Phys. Rev. A **97**, 063804 (2018).
11. S. Sofer, E. Strizhevsky, A. Schori, *et al.*, "Quantum enhanced x-ray detection," Phys. Rev. X **9**, 031033 (2019).
12. N. Hartley, D. Hodge, T. Buckway, *et al.*, "Confirming X-ray parametric down conversion by time–energy correlation," Results Phys. **57**, 107328 (2024).
13. J. C. Goodrich, R. Mahon, J. Hanrahan, *et al.*, "Quantum imaging with x-rays," arXiv (2024).
14. I. Freund and B. F. Levine, "Parametric conversion of X rays," Phys. Rev. Lett. **23**, 854 (1969).
15. B. Levine and I. Freund, "Parametric down conversion of x-rays," Opt. Commun. **1**, 419–422 (1970).
16. Y.-R. Shen, *Principles of Nonlinear Optics* (Wiley-Interscience, 1984).
17. P. Eisenberger and S. L. McCall, "X-ray parametric conversion," Phys. Rev. Lett. **26**, 684 (1971).
18. R. Schuetzhold, G. Schaller, and D. Habs, "Tabletop creation of entangled multi-keV photon pairs and the Unruh effect," Phys. Rev. Lett. **100**, 091301 (2008).
19. A. Pálffy, C. H. Keitel, and J. Evers, "Single-photon entanglement in the keV regime via coherent control of nuclear forward scattering," Phys. Rev. Lett. **103**, 017401 (2009).
20. L. Zhang, Z. Z. Li, D. Liu, *et al.*, "Entangled x-ray photon pair generation by free-electron lasers," Phys. Rev. Lett. **131**, 073601 (2023).
21. D. Borodin, A. Schori, F. Zontone, *et al.*, "X-ray photon pairs with highly suppressed background," Phys. Rev. A **94**, 013843 (2016).
22. H. N. Chapman, C. Caleman, and N. Timneanu, "Diffraction before destruction," Philos. Trans. R. Soc. Lond. B **369**, 20130313 (2014).
23. M. Mo, S. Murphy, Z. Chen, *et al.*, "Visualization of ultrafast melting initiated from radiation-driven defects in solids," Sci. Adv. **5**, eaaw0392 (2019).
24. M. Howells, T. Beetz, H. Chapman, *et al.*, "An assessment of the resolution limitation due to radiation-damage in X-ray diffraction microscopy," J. Electron Spectrosc. Relat. Phenom. **170**, 4–12 (2009).
25. C. K. Hong, Z. Y. Ou, and L. Mandel, "Measurement of subpicosecond time intervals between two photons by interference," Phys. Rev. Lett. **59**, 2044 (1987).
26. S. Volkovich and S. Shwartz, "Subattosecond x-ray Hong–Ou–Mandel metrology," Opt. Lett. **45**, 2728–2731 (2020).
27. S. Shwartz and S. E. Harris, "Polarization entangled photons at x-ray energies," Phys. Rev. Lett. **106**, 080501 (2011).
28. A. Eshun, O. Varnavski, J. P. Villabona-Monsalve, *et al.*, "Entangled photon spectroscopy," Acc. Chem. Res. **55**, 991–1003 (2022).
29. O. Varnavski, S. K. Giri, T.-M. Chiang, *et al.*, "Colors of entangled two-photon absorption," Proc. Natl. Acad. Sci. USA **120**, e2307719120 (2023).
30. R. W. Schoenlein, C. Adolphsen, R. A. Mori, *et al.*, "LCLS-II high energy (LCLS-II-HE): a transformative X-ray laser for science," Tech. Rep. SLAC-R-1143 (SLAC National Accelerator Laboratory (SLAC), 2016).
31. S. Sofer, O. Sefi, E. Strizhevsky, *et al.*, "Observation of strong nonlinear interactions in parametric down-conversion of X-rays into ultraviolet radiation," Nat. Commun. **10**, 5673 (2019).

32. M. Yabashi, H. Tanaka, K. Tono, *et al.*, "Status of the SACLA facility," Appl. Sci. **7**, 604 (2017).

33. S. H. Glenzer and R. Redmer, "X-ray Thomson scattering in high energy density plasmas," Rev. Mod. Phys. **81**, 1625 (2009).

34. E. Strizhevsky, D. Borodin, A. Schori, *et al.*, "Efficient interaction of heralded x-ray photons with a beam splitter," Phys. Rev. Lett. **127**, 013603 (2021).

35. Y. Klein, E. Strizhevsky, H. Aknin, *et al.*, "X-ray phase measurements by time-energy correlated photon pairs," arXiv (2024).